Int. J. Electrochem. Sci., 14 **(2019)** 5143 – 5153, doi: 10.20964/2019.06.58

International Journal of
ELECTROCHEMICAL
SCIENCE
www.electrochemsci.org

Growth of a Cu(Co) film by underpotential deposition of Co and controlling the time of the surface-limited redox replacement of Cu

J.S. Fang[1,*], *H.M. Wang*[1], *C.H. Hsu*[1], *Y.L. Cheng*[2], *G.S. Chen*[3]

[1] Department of Materials Science and Engineering, National Formosa University, Huwei, 63201 Yunlin, Taiwan
[2] Department of Electrical Engineering, National Chi-Nan University, Nan-Tou 64561, Taiwan
[3] Department of Materials Science and Engineering, Feng Chia University, Taichung 40724, Taiwan
[*]E-mail: jsfang@nfu.edu.tw

Received: 6 February 2019 / *Accepted:* 2 April 2019 / *Published:* 10 May 2019

Alternating between the underpotential deposition (UPD) of Co and surface-limited redox replacement (SLRR) of Cu enables the growth of a Cu(Co) film in a layer-by-layer manner. The technique is essential for fabricating Cu interconnects in nano-sized microelectronics. This work presents a technique to control the composition of a Cu(Co) film by controlling the time of the open circuit potential (OCP) during the SLRR of Cu because a longer OCP time results in a greater replacement of the UPD-Co by Cu^{2+}. The results of this work further show that the addition of H_3BO_3 to the Co electrolyte enhances the deposition of UPD-Co without the formation of $Co(OH)_2$. The crystalline structure of the resultant film is examined by X-ray diffraction to confirm the formation of the Cu(Co) film. The effect of the addition of H_3BO_3 to the Co electrolyte on the formation of the Cu(Co) film via the proposed process is demonstrated.

Keywords: Cu(Co) film, underpotential deposition, surface-limited redox replacement, Cu interconnections

1. INTRODUCTION

Conventional Cu interconnects are fabricated by a sequence of electrodepositing a Cu film on a stacked layer of Cu seeds and a Ta/TaN barrier. Both the Cu seeds and Ta/TaN barrier are normally deposited by sputtering. However, scaling down the feature size of a device makes the conformal deposition of the sputtered Ta/TaN barrier and Cu seeds an issue. Hence, developing a method for film deposition in a conformal growth manner is essential for preserving the integrity of Cu interconnect processes.

Alternatively, Cu alloy films are an emerging Cu-barrier technology that eliminates the use of conventional Ta/TaN barriers [1]. Among the alloying elements in a Cu alloy film, Co is a noncompound-forming element in the Cu matrix [2]. Additionally, the gap filling capability of Cu electrodeposition can be enhanced by the presence of a Co liner in nanoscale interconnect structures because the Co provides better wetting for the electrodeposition of Cu [3,4]. Thus, alloying Cu films with Co as the liner can potentially improve the wettability of the subsequent Cu electrodeposition and extend the use of the Cu interconnect [5-7]. Cu(Co) thin films have been conventionally used for applications in magnetic data recording and magnetic sensing based on their giant magnetoresistance effect [8-9]. In the electrodeposition process of Cu(Co) films, the concentration of Cu2+ and Co2+ in the electrolyte, pH value, and current density vary the compositions of the resulting films [10-12]. However, the more noble Cu is preferentially deposited from the mixed Cu-Co electrolyte, making compositional control of Cu and Co more difficult. Furthermore, Co dissolves easily in conventional acidic Cu electrolytes due to galvanic corrosion [13]. Thus, including an additive in the electrolyte for the electrodeposition of a Cu(Co) film is essential for avoiding Co dissolution and improving the composition control [1, 14-16].

Much attention has been paid in the literature on Cu(Co) alloy films deposited by conventional electrodeposition or electrochemical codeposition methods [15-18]; no information is available on the underpotential deposition (UPD) of Co to mediate the growth of a Cu(Co) film in the subsequent surface-limited redox replacement (SLRR) of Cu. This process, in turn, can manipulate the concentration of the films by controlling the time of the open circuit potential (OCP) during the Cu-SLRR. The standard potential difference of Cu/Co makes Co a suitable mediated layer [19-21].

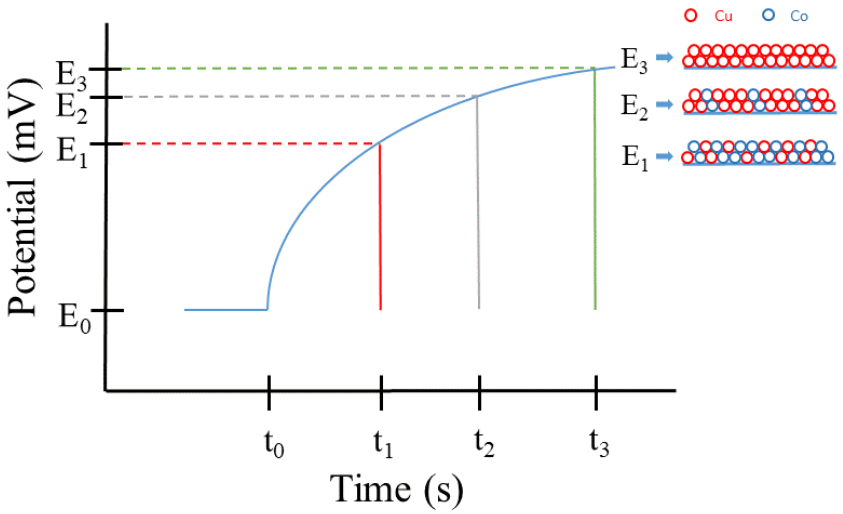

Figure 1. Single-cycle schematic of Co-UPD at E_0 followed by OCP for the Cu-SLRR that had been terminated at certain times of t_1, t_2, and t_3, corresponding to the terminated potentials of E_1, E_2, and E_3, respectively.

As proposed in the schematic shown in Fig. 1, E_0 is the potential for Co-UPD, and E_1 is the potential for the Cu-SLRR terminated at a certain OCP time. In this process, the Cu^{2+} in the electrolyte only replaces a portion of the UPD-Co adatoms and forms a controlled concentration in the Cu(Co) layer.

Increasing the OCP time (terminating at a potential of E_2) can produce a Cu(Co) layer with a higher concentration of Cu due to the Cu^{2+} in the electrolyte replacing a greater portion of the UPD-Co. In the case of the Cu-SLRR potential being terminated at an equilibrium potential of E_3, Cu^{2+} can completely replace the UPD-Co. Through these processes, varied concentrations of Cu(Co) films can be obtained by controlling the OCP time during the Cu-SLRR. This process can bring renewed interest in microelectronics with Cu interconnections.

2. EXPERIMENTAL PROCEDURES

The Cu(Co) film was prepared on a Si substrate coated with Au (50 nm)/Ti (3 nm). The Au film was deposited by direct current sputtering at a power of 20 W, and the Ti was deposited by radio frequency sputtering at a power of 100 W. The working pressure for the sputtering was 0.53 Pa of Ar. Both the UPD and SLRR processes were performed at room temperature in a deposition cell. The Au (50 nm)/Ti (3 nm)/Si substrate had a plate size of 1.9 cm × 1.9 cm. The deposition cell used this substrate as the working electrode, a gold wire as the auxiliary electrode, and Ag/AgCl as the reference electrode (3 M KCl, Bioanalytical Systems Inc.). The deposition potential was determined using a potentiostat (Metrohm Autolab PGSTAT101). A sacrificial Co monolayer (ML) was first deposited via UPD at a potential range between -900 mV and -930 mV, which was determined from the cyclic voltammetry (CV) scans of a Co electrolyte at a scan rate of 10 mV/s. The Co electrolyte was prepared by mixing 1.0 mM $CoSO_4 \cdot 7H_2O$ (Hayashi Pure Chemical) with varying concentrations of H_3BO_3 (Wako Pure Chemical Industries) that ranged from 0 to 5 mM. During the process, the Co electrolyte was pumped into the deposition cell and maintained for 60 s at the chosen potential to form the UPD-Co layer. Then, deionized water was pumped into the deposition cell to remove the existing Co electrolyte and rinse the deposition cell. Afterwards, the Cu electrolyte was pumped into the deposition cell at the OCP and the Cu-SLRR was allowed to occur by replacing the UPD-Co for a controlled amount of time between 20 s and 300 s based on the standard potential values difference between Cu and Co (E_0 Cu/Cu^{2+} = +340 mV/SHE, E_0 Co/Co^{2+} = -280 mV/SHE). The Cu electrolyte was a mixture of 1.0 mM $CuSO_4 \cdot 5H_2O$ (Hayashi Pure Chemical) and 0.7 mM $C_2H_4(NH_2)_2$ (Shimakyu's Pure Chemical). The Cu(Co) films were then deposited by sequentially performing the UPD-Co and the SLRR-Cu processes in the respective electrolytes with different OCP times for 50 cycles of the Cu-SLRR. Deionized water was deoxygenated for one hour with high purity nitrogen before use to minimize the dissolved oxygen content in the water.

The crystalline structure of the film was analyzed by X-ray diffractometry (XRD) with Cu Kα radiation on a Bruker AXS D8A25 system. The compositions of the Cu(Co) films were determined by energy dispersive spectroscopy (EDS, Oxford INCA PnetalFETx3). An adhesion test machine (Romulus III-A Universal Materials Tester) was used to measure the adhesion strength of Cu(Co) to the substrate at a constant pulling force of 100 kg. Before the adhesion test, a pin with a diameter of 0.27 cm was attached to the Cu(Co) film using resin, followed by heating at 150°C for 1.5 h to ensure adhesion between the resin and the Cu(Co) film.

3. RESULTS AND DISCUSSION

To determine the reductive potentials of the Co electrolytes with different added concentrations of H_3BO_3, CV scans at 10 mV/s were first carried out in a scanning range of +200 mV to -1300 mV. The results of the CV scans are shown in Fig. 2.

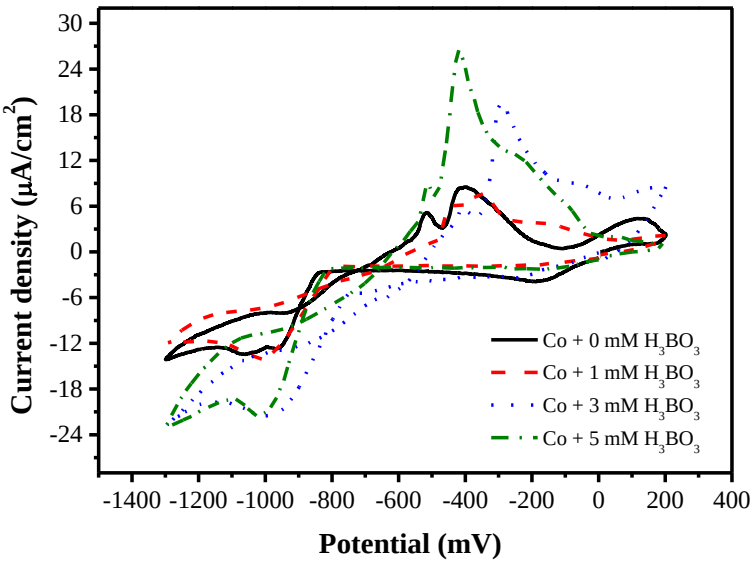

Figure 2. Cyclic voltammograms for the Au/Ti/Si substrate in the 1.0 mM $CoSO_4 \cdot 7H_2O$ electrolytes with various H_3BO_3 additions (concentrations of 0 mM, 1 mM, 3 mM, and 5 mM) at a scan rate of 10 mV/s.

As shown, the reductive current density obtained for the electrolyte without the addition of H_3BO_3 begins to increase significantly at -840 mV, followed by two tiny reductive potential peaks appearing at -980 mV and -1080 mV. The reductive potential at -980 mV was attributed to the reduction of Co and that at -1080 mV was related to the reduction of $Co(OH)_2$ [22]. The further increase in the current density after scanning at potentials lower than -1200 mV was associated with the hydrogen evolution reaction. This explained the formation of $Co(OH)_2$ because the present OH^- may react with Co^{2+} in the electrolyte. The results obtained from the CV scans showed that the reductive potential of the Co electrolyte was -1000 mV for 1 mM H_3BO_3, -1000 mV for 3 mM H_3BO_3, and -1020 mV for 5 mM H_3BO_3. The reductive potential of the Co electrolyte slightly increased with the addition of H_3BO_3. The electrolyte with added H_3BO_3 also increased the reductive current density during the CV scans, indicating that the deposition of Co can be improved by the addition of H_3BO_3. Santos et al. [23] showed that hydrogen generation in a Co electrolyte at a certain negative potential is accompanied by the formation of OH^- in the vicinity of the electrode during the electrodeposition. The presence of OH^- increases the pH value near the electrode and therefore affects the film deposition. This phenomenon can be compensated for by the addition of H_3BO_3 to the electrolyte because H_3BO_3 dissociation can generate H^+ to offset the OH^- near the electrode. However, no reduction of $Co(OH)_2$ was found when H_3BO_3 was added to the Co electrolyte because H_3BO_3 can prevent the formation of hydroxide

compounds[24-25]. Thus, the addition of H_3BO_3 in this study could prevent the formation of $Co(OH)_2$, which will be discussed with the results of the structural analysis of the films. The UPD occurs at a deposition potential prior to the formal reductive potential. From the CV results shown in Fig. 2, the deposition potential of UPD-Co occurred at -900 mV for 0 mM H_3BO_3, -910 mV for 1 mM H_3BO_3, -930 mV for 3 mM H_3BO_3, and -930 mV for 5 mM H_3BO_3.

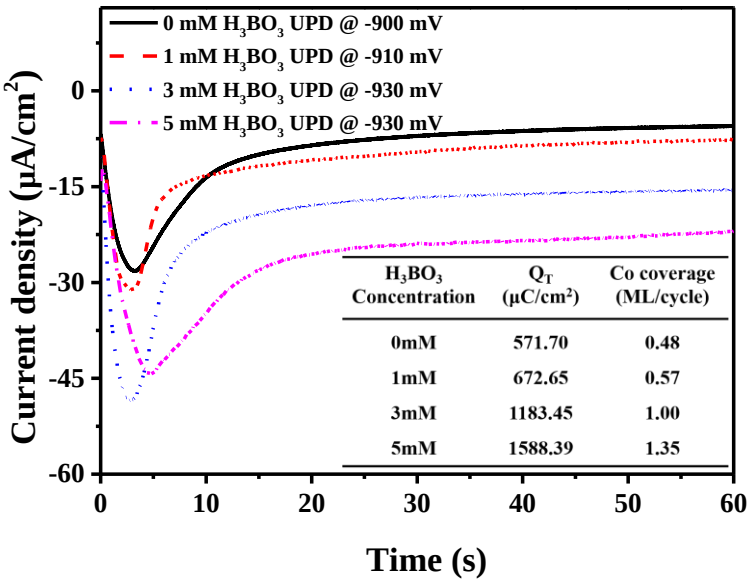

Figure 3. Current-time curves for the UPD-Co recorded for H_3BO_3 concentrations of 0 mM, 1 mM, 3 mM, and 5 mM in the 1.0 mM $CoSO_4 \cdot 7H_2O$ electrolyte. The inset table shows the electrical charge and Co coverage for single-cycle deposition.

The current-time curve of the Co-UPD was used to determine the coverage of the UPD-Co. Figure 3 shows the measured transient current density versus time curves that were recorded during the respective UPD of Co for the Co electrolytes with different H_3BO_3 concentrations. Initially, the current density dramatically increases to a negative value and then reaches a maximum negative value. In this stage, the applied potential of UPD causes the reduction of Co^{2+} and forms a Co adlayer on the substrate. Subsequently, the current density decreased gradually until reaching a stable value. The stable curve indicated that the UPD of Co had been terminated due to UPD occurring at potentials prior to the potential for bulk deposition. The maximum current density occurred after 3 s for the Co electrolytes with H_3BO_3 concentrations of less than 3 mM. However, the time to reach the maximum current density for the 5 mM H_3BO_3 was slightly increased to 5 s, which may have been due to the higher reductive potential of the electrolyte with higher added H_3BO_3 concentrations [15-17]. Integration of the current density-time curves shown in Fig. 3 could provide the deposition charge of the UPD-Co for the respective Co electrolyte. The deposition charges are summarized in the table inset in Fig. 3. These charges were divided by 2 owing to two electrons being transferred when one Co adatom was replaced by one Cu^{2+} ion. Additionally, the formation of one Co monolayer requires a charge of 590 $\mu C/cm^2$ [26]. Thus, the respective charge obtained yields the coverage of the UPD-Co. The Co coverage was in the

range of 0.48 ML and 1.35 ML for the Co-UPD. The obtained coverage confirms the UPD-Co, which approximately deposited a monolayer because the deposition potential occurred prior to the formal reductive potential. The table inset also shows that the UPD-Co coverage increased with increasing concentration of H_3BO_3, suggesting that H_3BO_3 promoted the UPD-Co.

Next, the Cu electrolyte was introduced to the cell to replace the existing UPD-Co layer through the Cu-SLRR at the OCP. Figure 4 shows the potential-time curves for the replacement of UPD-Co by Cu^{2+} recorded during the OCP for 300 s. In this SLRR process, the reductive potential difference between Cu and Co initiates the replacement between the Cu^{2+} in the electrolyte and the UPD-Co. During the replacement, the potential increased continuously until reaching a negative potential, and subsequently decreased to a stable potential when the replacement had completed. A high UPD-Co coverage generally required a long replacement time. Thus, 0 mM and 1 mM H_3BO_3 had the lowest UPD-Co coverage and therefore resulted in the shortest replacement times to reach the stable potential. However, the potential still increased slightly when the OCP was 300 s during the Cu-SLRR for the Co electrolyte with added H_3BO_3. This fact may indicate that the UPD-Co had not been completely replaced by Cu^{2+} due to the H_3BO_3 addition causing high coverage of the UPD-Co adlayer. Note that the current density transient with time (not shown) also showed a similar tendency as that of the potential transient with time. The current density increased significantly at the beginning until reaching a maximum negative value (from ~ -30 μA/cm^2 for the 0 mM H_3BO_3 addition to ~ -45 μA/cm^2 for the 5 mM H_3BO_3 addition) and then decreased to a stable current density (from ~ -5 μA/cm^2 for the 0 mM H_3BO_3 addition to ~ -20 μA/cm^2 for the 5 mM H_3BO_3 addition) when the replacement had completed.

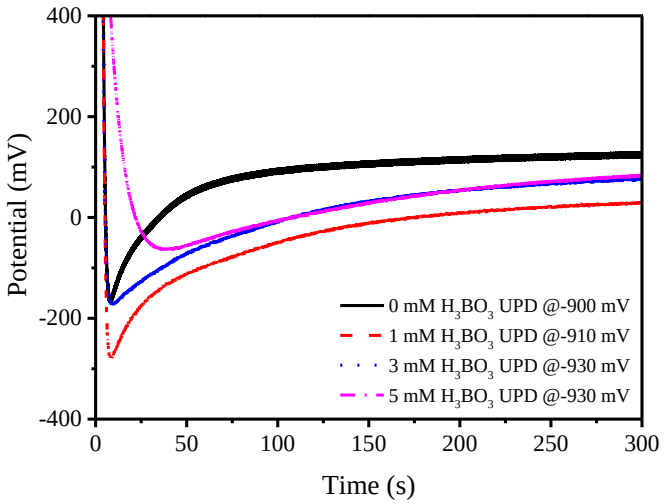

Figure 4. Potential-time curves for the Cu-SLRR of the UPD-Co deposited substrates in the 1.0 mM $CoSO_4 \cdot 7H_2O$ electrolyte with the addition of 0 mM, 1 mM, 3 mM, and 5 mM H_3BO_3.

As the potential-time curves show in Fig. 4, the replacement of UPD-Co by the Cu^{2+} in the electrolyte during the SLRR process was closely related to the OCP time. A longer OCP time caused greater replacement and resulted in a higher Cu concentration in the Cu(Co) film. Thus, the composition of the Cu(Co) film could be controlled by manipulating the OCP time during the SLRR process. Figure

5 shows the Cu/Co composition ratios of the resultant Cu(Co) films that were deposited at the respective Co-UPD potential with the SLRR process having been terminated at different OCP times. As shown, the Cu/Co composition ratio increased with increasing OCP time. Additionally, the higher concentrations of H_3BO_3 in the Co electrolyte caused greater Co coverage (shown in the table inset in Fig. 3); thus, H_3BO_3 induced a lower Cu/Co composition ratio in the Cu(Co) film. The results shown in Fig. 5 indicate that the composition of the Cu(Co) film could be adjusted simply by controlling the OCP time during the Cu-SLRR.

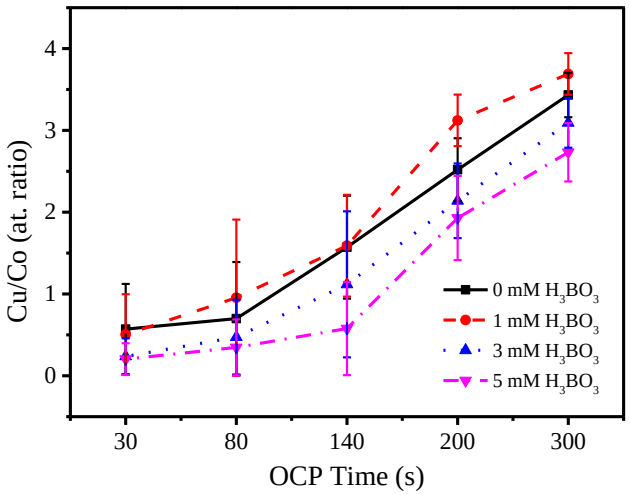

Figure 5. Composition ratios of Cu/Co for the Cu(Co) films deposited for certain OCP times during the Cu-SLRR.

Figure 6 shows the XRD results of the Cu(Co) films that were deposited at the respective Co-UPD with different OCP for the Cu-SLRR. A progressive shift of the diffraction peak to lower diffraction angles was observed as the OCP time increased, suggesting an increase in the Cu content of the Cu(Co) film. The Cu(Co) film that was deposited without the addition of H_3BO_3 had a Co (111) diffraction peak ($2\theta = 44.3°$, JCPDS 05-0727) at OCP times of less than 100 s, as shown in Fig. 6a. The Co (111) peak gradually changes to a Cu (111) peak when the OCP time was longer than 100 s. As a result, the intensity of the Cu (111) peak ($2\theta = 43.2°$, JCPDS 89-2838) became stronger with longer OCP time. A longer OCP time tended to form more Cu (111), supporting the fact that Cu^{2+} replaced UPD-Co. Additionally, a tiny peak corresponding to the $Co(OH)_2$ (100) plane ($2\theta = 33.0°$, JCPDS 030-0443) was also found in the XRD patterns because of the generation of OH^- during the Co-UPD. Figure 6b shows the XRD result of the Cu(Co) film that was prepared in the UPD-Co electrolyte with a 1 mM H_3BO_3 addition. The Co (111) peak can be found at short OCP time points, and the diffraction peak became significant as the OCP time increased beyond 140 s. With the 3 mM (Fig. 6c) and 5 mM (Fig. 6d) additions of H_3BO_3, the formation of the Cu (111) peak was also found at longer OCP times. In addition, no diffraction peak for $Co(OH)_2$ was found when H_3BO_3 was added to the electrolyte, indicating that H_3BO_3 could prevent the formation of $Co(OH)_2$. The XRD results agree with the compositional findings shown in Fig. 5, indicating that the Cu content could be increased by extending the OCP time during the Cu-SLRR and allowing greater replacement between Cu^{2+} and the UPD-Co.

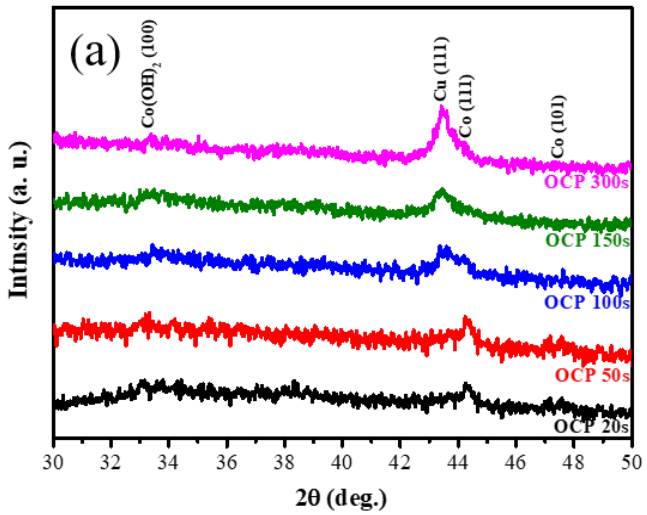
(a)
Co(OH)2 (100)
Cu (111)
Co (111)
Co (101)
OCP 300s
OCP 150s
OCP 100s
OCP 50s
OCP 20s
Intnsity (a. u.)
30 32 34 36 38 40 42 44 46 48 50
2θ (deg.)

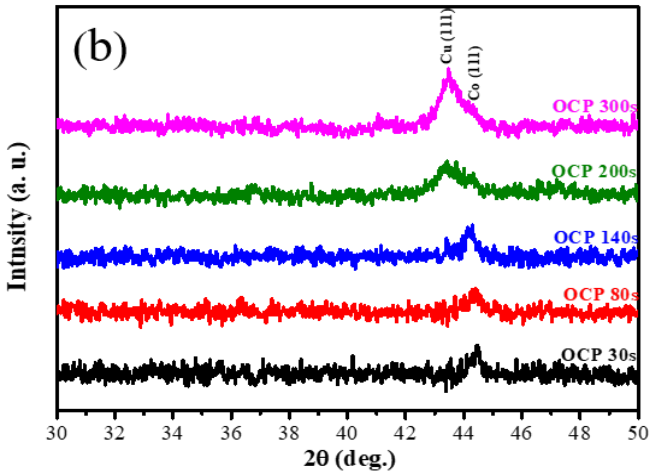
(b)
Cu (111)
Co (111)
OCP 300s
OCP 200s
OCP 140s
OCP 80s
OCP 30s
Intnsity (a. u.)
30 32 34 36 38 40 42 44 46 48 50
2θ (deg.)

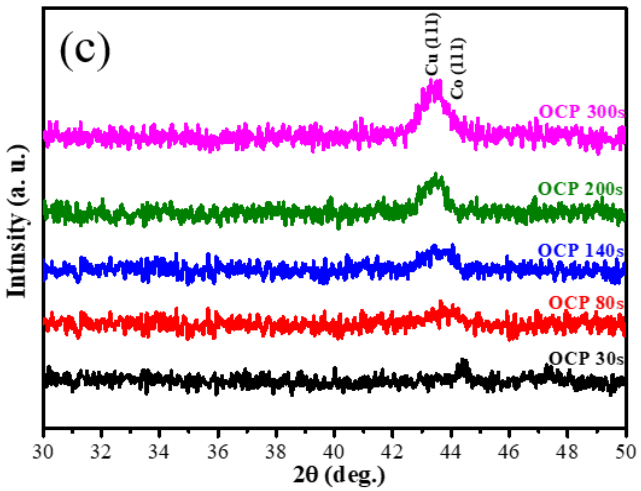
(c)
Cu (111)
Co (111)
OCP 300s
OCP 200s
OCP 140s
OCP 80s
OCP 30s
Intnsity (a. u.)
30 32 34 36 38 40 42 44 46 48 50
2θ (deg.)

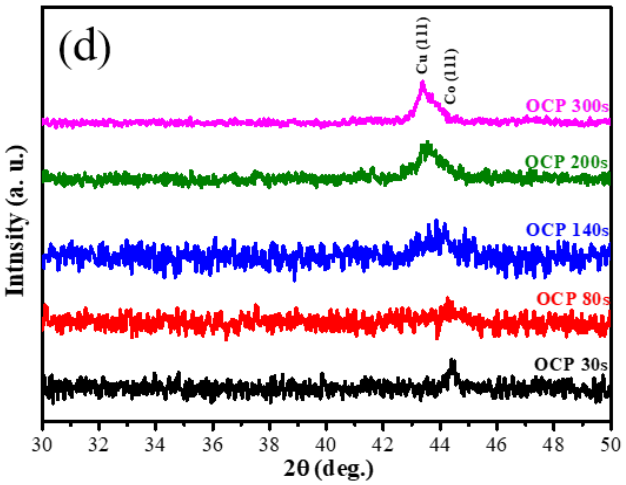

Figure 6. Structural results examined by XRD for the Cu(Co) films deposited for certain OCP times during the Cu-SLRR. The 1.0 mM $CoSO_4 \cdot 7H_2O$ electrolyte for the UPD had various H_3BO_3 concentrations of (a) 0 mM, (b) 1 mM, (c) 3 mM, and (d) 5 mM.

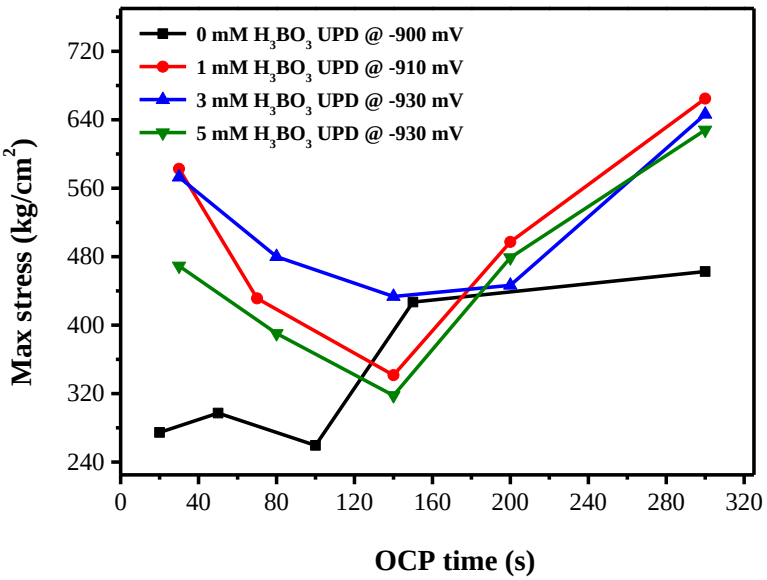

Figure 7. Adhesion results for the Cu(Co) films deposited via UPD-Co with 0 mM, 1 mM, 3 mM, and 5 mM concentrations of H_3BO_3 and terminated at a certain OCP time during the Cu-SLRR.

The adhesion of the resultant Cu(Co) films onto the substrate was investigated by a peeling test. As shown in Fig. 7, the adhesion strength tended to decrease initially with increasing OCP times up to140 s, followed by increasing adhesion strength as the OCP time increased to 300 s. The films deposited with the addition of H_3BO_3 seemed to have increased adhesion strengths. However, the adhesions were approximately the same when the film was deposited for longer OCP times, except for

the Cu(Co) film prepared with the Co electrolyte without the addition of H_3BO_3. As discussed, a shorter OCP time resulted in a higher Co content in the Cu(Co) films. The adhesion strongly depended on both the H_3BO_3 addition and the OCP time. The highest adhesion strengths, which were greater than 640 kg/cm^2, were achieved for the Cu(Co) films deposited in the electrolytes with added H_3BO_3 at an OCP time of 300 s for the Cu-SLRR. For the sample without the H_3BO_3 addition, the low adhesion strength might be due to the formation of $Co(OH)_2$, which formed at the hydrogen generation potential. The formed hydrogen could be adsorbed onto the surface of the substrate to buffer the incoming Cu^{2+} [27-28]. This could induce a more porous structure in the film and reduce the adhesion of the Cu(Co) film to the substrate. However, the OCP time of 140 s had a lower adhesion strength, which may be due to an inappropriate mixture of Cu and Co that resulted in a high lattice mismatch in the Cu(Co) film. The lattice mismatch, therefore, reduced the bonding between the Cu(Co) film and the substrate [29].

4. CONCLUSIONS

An electrochemical layer-by-layer deposition method for a Cu(Co) film was demonstrated. The technique was initiated by Co-UPD followed by Cu-SLRR. By controlling the OCP time during the Cu-SLRR, the composition of the resultant Cu(Co) film could be adjusted according to the replacement of the UPD-Co by Cu^{2+}. The coverage of UPD-Co could be significantly improved by the addition of H_3BO_3 to the Co electrolyte because of the resulting absence of $Co(OH)_2$. The addition of H_3BO_3 further enhanced the adhesion of the Cu(Co) film to the substrate. The proposed technique may be useful in the electrochemical deposition of Cu(Co) films in a layer-by-layer manner for applications in Cu interconnects in future microelectronics.

ACKNOWLEDGEMENT
This work is financially supported by the Ministry of Science and Technology, Taiwan under the grant MOST 107-2221-E-150-002-MY2. We also thank the experimental support from the Common Laboratory for Micro/Nano Science and Technology of National Formosa University.

References

1. B.R. Tzaneva, A.I. Naydenov, S.Zh. Todorova, V.H. Videkov, V.S. Milusheva, P.K. Stefanov, *Electrochim. Acta*, 191 (2016) 192.
2. K. Barmak, C. Cabrai. Jr, P. Rodbell, J.M.E. Harper, *J. Vac. Sci. Technol.*, B 24 (2006) 2485.
3. M. He, X. Zhang, T. Nogami, X. Lin, J. Kelly, H. Kim, T. Spooner, D. Edlstein, L. Zhao, *J. Electrochem. Soc.*, 160 (2013) D3040
4. X. Zhang, L. Cao, V. Ryan, P.S. Ho, B. Tayler, C. Witt, C. Labelle, *ECS J. Solid State Technol.*, 4 (2015) N3177.
5. S.H. Sung, J. Chawla, C. Carver, R. Chebiam, J. Clarke, C. Jezewski, T. Tronic, R.B. Turkot, H.J. Yoo, *IITC*, (2015) pp.87.
6. D. Gall, *J. Appl. Phys.*, 119 (2016) 085101.
7. J.S. Chawla, S.H. Sung, S.A. Bojarski, C.T. Carver, M. Chandhok, R.V. Chebiam, J.S. Clarke, M. Harmes, C.J. Jezewski, M.J. Kobrinski, B.J. Krist, M. Mayeh, R. Turkot, H.J. Yoo, *IITC/AMC*,

(2016) pp. 63.
8. M. del C. Aguirre, H. Núñez Coaras, L.M. Fabietti, S.E. Urreta, *J. Phys. Chem.*, C 120 (2016) 22142.
9. C. Reig, M. Cubells-Beltran, D.R. Muñoz, *Sensors*, 9 (2009) 7919.
10. G.R. Pattanaik, D.K. Pandya, S.C. Kashyap, *J. Electrochem. Soc.*, 149 (2002) C363.
11. H.J. Blythe, V.M. Fedosyuk, *Phys. Status Solidi.*, A 146 (1994) K13.
12. S. Ge, H. Li, C.Li, L. Xi, J. Chi, *J. Phys.: Condens. Matter.*, 12 (2000) 5905.
13. J. Horkans, *J. Electrochem. Soc.*, 126 (1979) 1861.
14. K.M. Yin, B.T. Lin, *Surf. Coating & Technol.*, 78 (1996) 205.
15. A. Vicenzo, P. L. Cavallotti, *Electrochim. Acta*, 49 (2004) 4079.
16. J. Dille, J. Charlier, R. Winand, *J. Mater. Sci.*, 32 (1997) 2637.
17. R.Sivasubramanian, M.V.Sangaranarayanan, *Mater. Chem. & Phy.*, 136 (2012) 447.
18. T.G. de Lima, B.C.C.A. Rocha, A.V.C. Braga, D.C.B. do Lago, A.S. Luna, L.F. Senna, *Surf. Coatings & Technol.*, 276 (2015) 606.
19. J.P. Hoare, *J. Electrochem. Soc.*, 133 (1986) 2491.
20. B.V. Tilak, A.S. Gendron, M.A. Mosoiu, *J. Appl. Electrochem.*, 7 (1977) 485.
21. A.J. Bard, L.R. Faulkner, *Electrochemical methods Fundamentals and Applications*, Wiley, (2001) pp.808.
22. C.Q. Cui, S. P. Jiang, A. C. C. Tseung, *J. Electrochem. Soc.*, 137 (1990) 3374.
23. J.S. Santos, R. Matos, F. Trivinho-Strixino, E.C. Pereira, *Electrochim. Acta*, 53 (2007) 644.
24. D.R. Gabe, *J. Appl. Electrochem.*, 27 (1997) 908.
25. M. Rojas, C.L. Fan, H.J. Miao, D.L. Piron, *J. Appl. Electrochem.*, 22 (1992) 1135.
26. L.H. Mendoza-Huizar, J. Robles, M. Palomar-Pardave, *J. Electroanal. Chem.*, 521 (2002) 95.
27. D. Grujicic, B. Pesic, *Electrochim. Acta*, 49 (2004) 4719.
28. J. Lu, D. Dreisinger, T. Glück, *Hydrometallurgy*, 178 (2018) 19 .
29. N. Okamoto, F. Wang, T. Watanabe, *Mater. Trans.*, 45 (2004) 3330.